Analytical Biochemistry 684 (2024) 115374

Contents lists available at ScienceDirect

Analytical Biochemistry

journal homepage: www.elsevier.com/locate/yabio

Direct competitive assay for HER2 detection in human plasma using Bloch surface wave-based biosensors

Tommaso Pileri [a], Alberto Sinibaldi [a,b,*], Agostino Occhicone [a,b], Norbert Danz [c], Elena Giordani [d], Matteo Allegretti [d], Frank Sonntag [e], Peter Munzert [c], Patrizio Giacomini [d], Francesco Michelotti [a,b]

[a] SAPIENZA Università di Roma, Department of Basic and Applied Sciences for Engineering, Via A. Scarpa, 16, 00161, Roma, Italy
[b] Center for Life Nano and Neuro Science, Italian Institute of Technology (IIT), Viale Regina Elena 291, 00161, Rome, Italy
[c] Fraunhofer Institute for Applied Optics and Precision Engineering, A.-Einstein-Str. 7, 07745, Jena, Germany
[d] Translational Oncology Research Unit, IRCCS Regina Elena National Cancer Institute, Rome, Italy
[e] Fraunhofer Institute for Material and Beam Technology IWS, Winterbergstr. 28, 01277, Dresden, Germany

A R T I C L E I N F O

Keywords:
HER2
Biosensors
Biomarker
Photonic crystals
Bloch surface waves

A B S T R A C T

The overexpression and/or amplification of the HER2/neu oncogene has been proposed as a prognostic marker in breast cancer. The detection of the related peptide HER2 remains a grand challenge in cancer diagnosis and for therapeutic decision-making. Here, we used a biosensing device based on Bloch Surface Waves excited on a one-dimensional photonic crystal (1DPC) as valid alternative to standard techniques. The 1DPC was optimized to operate in the visible spectrum and the biosensor optics has been designed to combine label-free and fluorescence operation modes. This feature enables a real-time monitoring of a direct competitive assay using detection mAbs conjugated with quantum dots for an accurate discrimination in fluorescence mode between HER2-positive/negative human plasma samples. Such a competitive assay was implemented using patterned alternating areas where HER2-Fc chimera and reference molecules were bio-conjugated and monitored in a multiplexed way. By combining Label-Free and fluorescence detection analysis, we were able to tune the parameters of the assay and provide an HER2 detection in human plasma in less than 20 min, allowing for a cost-effective assay and rapid turnaround time. The proposed approach offers a promising technique capable of performing combined label-free and fluorescence detection for both diagnosis and therapeutic monitoring of diseases.

1. Introduction

During the last two decades, biosensors were widely used as the most reliable, fast, and precise analytical tools in cancer biomarkers detection worldwide [1]. Indeed, to actively recognize tumor, biosensors make use of various biorecognition elements such as antibodies, enzymes, single strand deoxyribonucleic acid (ssDNA), cancer cells, nucleic acid probes (aptamers) or other biomolecules which are immobilized on a transducer surface. The latter can transform biological signals obtained from the interaction between target biomarker and probe molecules into measurable signals either electrical or optical [2–4]. For example, optical biosensors based on photonic crystals were extensively used by academicians, reaching sometimes pre-clinical environments [5–8]. Among them, one dimensional photonic crystals (1D-PCs) recently gained the attention of clinicians for their unique features: high sensitivities, capability to enhance fluorescence signals, improved turnaround time for results, low-cost fabrication issues [9–17]. Nevertheless, a reliable identification of cancer biomarkers at low concentrations in human body fluids, the so-called early disease detection, remains a challenge for academicians and clinicians. This crucial aspect would enormously support a more precise assignment of therapies to the patients with a net improvement in terms of efficacy of treatments, monitoring of the follow-up and a reduction of the costs.

The present work wants to address the points raised above suggesting a new optical approach based on new detection protocols on 1D-PC for breast cancer biomarker detection. Worldwide, breast cancer is the most common type of cancer diagnosed in women, occurring at a rate of about 25 % of cancer incidence, making such a disease one of the leading cancer-related mortality in women [18]. Among several breast cancer biomarkers, Human Epidermal Growth Factor Receptor 2 (HER2) is

* Corresponding author. SAPIENZA Università di Roma, Department of Basic and Applied Sciences for Engineering, Via A. Scarpa, 16, 00161, Roma, Italy.
E-mail address: alberto.sinibaldi@uniroma1.it (A. Sinibaldi).

https://doi.org/10.1016/j.ab.2023.115374
Received 20 June 2023; Received in revised form 13 October 2023; Accepted 29 October 2023
Available online 31 October 2023

routinely assessed in tumor tissues [1], most often from primary but also from metastatic tumors. When amplified/overexpressed HER2 may be targeted by therapeutic antibodies, both naked and conjugated with cytotoxic payloads [19].

The established diagnostic tests aimed to assess semi quantitatively the HER2 expression levels by immunohistochemistry (IHC) and fluorescent in situ hybridization (FISH) methods in surgically removed tissues and biopsies [20]. These techniques are invasive, expensive, require complex procedures and are time consuming. HER2 phenotyping in peripheral blood is in principle attractive but is not routine practice.

Besides being minimally invasive, liquid biopsy (HER2 in plasma or serum samples) [21] is potentially attractive for monitoring disease course and response to treatment [22]. As widely shown in the literature [23–25], it is largely agreed that HER2 is shed after proteolytic cleavage at an extracellular iuxta-membrane site, in the form of a soluble protein in serum/plasma. Currently, the gold standard technique used to quantify HER2 in serum is based on an enzyme-linked immunosorbent assay (ELISA) with a cut-off concentration value of 15 ng/mL approved by FDA [23,26]. Indeed, plasma from normal blood donors contains between 5 and 10 ng/mL whereas HER2-positive advanced breast cancer patients may have up to several hundreds of ng/mL [27,28].

The approach presented in this work is conceptually different with respect to the non-competitive direct protocol recently reported by our authors [29] in which a limit of detection (LoD) of 0.6 ng/mL was obtained for HER2. The detection mechanism is based on the use of a 1D-PC sustaining a Bloch surface wave (BSW) [30–35] and is combined with a direct competitive assay, in which the human plasma samples were allowed to react with a detection anti-HER2 mAb conjugated with a quantum dot in a vial before being tested with the 1D-PC biochip. Moreover, the latter were patterned by means of a nano plotting system into arrays of regions of interest directly with the HER2-Fc chimera protein (SIG) and control regions consisting of biologically inert molecules (CTRL). As already reported in previous works [29,33], the output of sensors based on 1D-PC can be label-free or provide fluorescence, depending on the operating conditions. In particular, the introduction of quantum dots, which are spectrally compliant with the read-out scheme, permitted to acquire sharper fluorescence spectra via the BSW excitation [36–38]. Unlike direct sandwich assays, here the HER2-positive plasma samples showed low signal levels whereas large signals are expected for the HER2-negative plasma samples. This feature dramatically reduces the duration of the assay down to 20 min, providing a convenient, cost-effective, and ultrasensitive alternative that minimizes the disadvantages of conventional methodologies [39].

2. Materials and methods

2.1. Readout system and the biochip

Here we give a short description of the readout system and the photonic crystal design; comprehensive reports can be found in Refs. [29,40] respectively. The 1D-PC consists of a periodic multilayer structure composed of two and a half periods of SiO_2 ($d_1 = 275\ nm$, $n_L = 1.474 + j5 \times 10^{-6}$) and Ta_2O_5 ($d_2 = 120\ nm$, $n_H = 2.160 + j5 \times 10^{-5}$) (Fig. 1a). The multilayer stack is deposited using plasma ion-assisted deposition (PIAD) in a high vacuum chamber [41] onto a truncated prism-shaped substrate made of TOPAS®, which is a cyclic olefin copolymer (TOPAS5013LS, $n = 1.526$). A thin double layer of TiO_2 ($d_3 = 20\ nm$, $n_{H'} = 2.28 + j1.8 \times 10^{-3}$) and SiO_2 ($d_4 = 20\ nm$) caps the periodic stack. The refractive indices of all the materials are referenced to a wavelength of 670 nm. The device is designed to operate in two modes, Label-Free (LF) and Fluorescence (FLR) (Fig. 1b), and is equipped with two independent lasers diodes as light sources: $\lambda_{LF} = 670\ nm$ and $\lambda_{FLR} = 638\ nm$. Both light beams are collimated, TE polarized, and shaped to form a finite length stripe (6 mm). The user can switch between the two operation modes by using two programmable shutters (Sh elements in Fig. 1b). The excitation of Bloch Surface Waves (BSWs) occurs at the interface between the 1D-PC and the surrounding medium when the light is coupled to the dielectric stack at a specific angle and wavelength that resonantly matches the BSW dispersion under the condition of total internal reflection [42].

A CCD camera (Apogee Ascent, Sony ICX814, resolution 3388x2712 pixels) placed after a Fourier lens in the collection branch (FL in Fig. 1b) records two different types of light. When LF mode is running, the CCD camera collects the totally internal reflected light. The resulting image

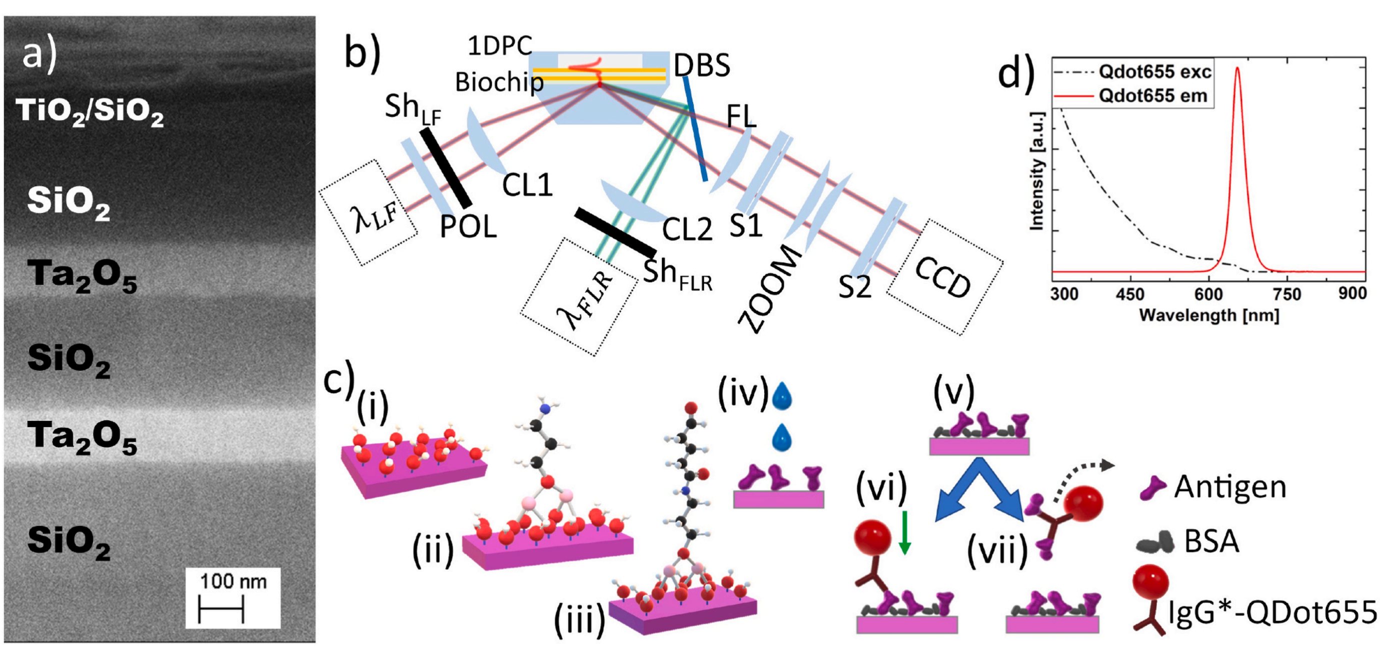

Fig. 1. (a) Scanning electron microscopy image of the 1D-PC cross-section with the multilayered structure. (b) Sketch of the optical read-out system. (c) Scheme of the assay protocol. The three-step silanization process based on APTES-Glutaraldehyde includes: (i) piranha cleaning, (ii) surface coverage with APTES monolayer, (iii) glutaraldehyde crosslinking. The competitive bioassay layout is based on: (iv) HER2 printing/immobilization, (v) surface blocking with BSA and the two possible scenarios for either a (vi) negative or a (vii) positive sample. (d) Excitation and emission spectra of the inorganic Qdot655®.

represents the reflectance angular spectrum along the illuminated area. In contrast, in the FLR mode, the fluorescence emitted at the top surface of the photonic crystal is imaged onto the CCD. As demonstrated elsewhere [43,44], the FLR operation mode provides a larger resolution with respect to the LF operation mode. Conversely, the latter allows us to monitor the progress of the experiment in real-time [29].

The flow cell is manufactured using an injection molding process in two steps. Firstly, a hard polymer is injected into the mold to create the hard biochip cover with two holes for the inlet/outlet of the fluidic system. Moreover, the hard cover was designed to complement the biochip substrate by means of two pairs of clamps. Then, an elastomer fills the hard cover and carves a central microfluidic channel linking the inlet and the outlet. This second injection also forms o-rings at the top of the cell, ensuring proper sealing of the fluidic contacts when the chip is inserted into the optical readout system. When the flow cell is clamped to the biochip, the microfluidic channel matches with the illuminated stripe.

2.2. Surface chemistry

With the aim of covalently binding peptides as probes towards a specific biomarker, a surface silanization was performed onto the 1D-PC top layer. A piranha cleaning ($H_2O_2/H_2SO_4 = 1/3$ [vol] – H_2O_2 30 vol, H_2SO_4 purity 99 %, both from Sigma-Aldrich) was performed to remove any pollutant compound and to hydroxylize the surface (Fig. 1c(i)). After thoroughly rinsing with deionized (DI) water and drying, the silanization step follows. This was done by immersing the 1D-PC coated biochips in a 2 % (v/v) solution of APTES ((3-Aminopropyl)triethoxysilane – Sigma-Aldrich) in absolute ethanol (Sigma-Aldrich) for 1 h at room temperature (Fig. 1c(ii)). Sonication, rinsing with DI water and drying followed and a curing step (1 h, 70 °C) was carried out to evaporate the solvent while the APTES monolayer untwists. The third step involved binding of glutaraldehyde (GAH) on APTES (Fig. 1c(iii)). GAH is a homo-bifunctional crosslinker used to efficiently immobilize peptidic probes via amidic bond. The biochips were soak in a solution of 1 % (v/v) glutaraldehyde (Sigma-Aldrich) in 100 mM $NaHCO_3$ buffer in presence of 0.1 mM $NaCNBH_3$ (sodium cyanoborohydride, Sigma-Aldrich) for 1 h at room temperature. This step ended with a final sonication, rinsing with DI water and drying. The surface modified biochips were then stored in a desiccator for 2 h at least before usage. Such a protocol leads to the 1DPC surface coverage by a monolayer of APTES-GAH as reported in Ref. [45].

2.3. Bioassay protocol

The bioassay protocol used in this work is derived from a direct competitive assay. It relies on the initial immobilization onto the chemically functionalized surface of the biochip of the same HER2 biomarker we want to detect in the samples. This was achieved by nanoplotting a 100 $\mu g/mL$ solution of HER2 in PBS 1 × onto five separate regions along the sensing area of the 1D-PC using a non-contact microarray printer with a high precision printing system by GeSiM (25 μm accuracy, 650 pL per drop) (Fig. 1c(iv)). The immobilized HER2 was a synthetic Fc chimera reproduction of the wild-type HER2 extracellular domain (R&D Systems). Following the printing process, the biochip was incubated for 1.5 h at 4 °C in a mildly humidified incubator to prevent evaporation. After surface rinsing with PBS 1 × , the bioconjugation procedure was completed by saturating the remaining free GAH binding sites by incubating a 1 mg/mL blocking solution of bovine serum albumin (BSA, Sigma-Aldrich, Fig. 1c(v)).

In the assays, the samples were firstly let to react for 30 min at room temperature in vials with a titrated solution of HER2 specific detection IgG* antibodies (detection-IgG*) that were fluorescently labeled with a quantum-dot via a click-chemistry conjugation step (IgG*-Qdot655 kit form ThermoFisher Scientific, and emission spectra shown in Fig. 1d). Then the resulting solution was injected into the biochip. Therefore, the competition feature tested here is that of the labeled antibodies towards the HER2 (eventually) present into the sample and the HER2 immobilized onto the 1D-PC surface as a bio-selective probe. If HER2 is present in the sample, it will form a complex with the IgG*-Qdot655 and only the remaining IgG*-Qdot655 can be trapped at the surface (Fig. 1c(vi)), while the complexed form flows away (Fig. 1c(vii)).

Actually, in the assays reported here, the 1D-PC biochip was coupled to its microfluidic cell already at the end of the HER2 immobilization step. The blocking procedure with BSA was carried out by injecting the BSA solution directly in the biochip, with the purpose to monitor the blocking step by means of the LF signal.

2.4. Human plasma samples

Whole blood samples (10 mL each) were drawn from healthy donors (aged 24–65) in BD Vacutainer K_2EDTA tubes and processed within 1 h. Plasma was isolated by two successive rounds of centrifugation at 4 °C (2000×g for 20 min, and 13000×g for 10 min), and stored at −80 °C in single-use 2 mL aliquots until further manipulation. No freeze-thawing cycles were allowed. In all experiments performed to optimize the competitive assay, a dilution ratio of 1:10 in PBS 1 × buffer was applied. During this phase, we used one plasma sample tested negative for HER2 and, as assessed by a commercial (Thermofisher) ELISA assay, we artificially generated positive samples by spiking HER2-Fc chimera until the concentration reached 100 ng/mL.

At the end of the competitive assay calibration procedures, for the second experimental phase, it was possible to complete a measurement campaign in which one sample of human plasma ERBB2 positive (identified as pt#13) and 2 samples of human plasma ERBB2 negative (pool of negative plasmas) were used. The plasmas of all patients tested with the nanophotonic platform were previously characterized by ELISA and dPCR methodology.

3. Results and discussion

3.1. Execution of the competitive assays

The single determinant bioassay protocol described above relies on the affinity of the detection-IgG* towards the antigens simultaneously present at the surface of a biochip and eventually in the sample under investigation.

Once the surface of the 1D-PC biochip was patterned with the HER2-Fc chimera, the biochip was coupled to the microfluidic cover and mounted on the platform for the assays. As shown in Fig. 2a, the reflectance map recorded in LF mode in PBS 1 × at the beginning of the assay, shows a periodic shift of the BSW resonance position in correspondence of the regions where the HER2-Fc chimera was immobilized, therefore demonstrating the efficiency of the patterning step. By measuring the angular shift of the BSW resonance and making use of the sensitivity of the biochips to changes of the refractive index of the solution and of the estimation of the penetration depth of the BSW exponential tail inside the analyte (113 nm), we could estimate the surface density of the HER2-Fc chimera immobilized in the SIG regions [46,47]. We found that the HER2 mass surface coverage was 1140 pg/mm^2, in line with other assays carried out with similar biomolecules [29].

Fig. 2b shows the LF sensograms recorded in all regions during the incubation for 10 min of the 1 mg/mL blocking solution of BSA in PBS 1x (step v). The binding kinetics recorded highlight the different behavior of the two types of regions. The sensograms demonstrate that BSA was more extensively covalently bound to the bare 1D-PC surface in the absence of HER2. Following a washing step, where 180 μL of PBS 1 × were introduced into the microfluidics to eliminate excess BSA, the LF signal was allowed to stabilize to a residual shift $\Delta\theta_{BSA}$. The $\Delta\theta_{BSA}$ values indicated that almost twice the amount of BSA was bound to the CTRL regions compared to the SIG, due to the limited availability of GAH binding sites after the bioconjugation step (iv). To quantify non-specific

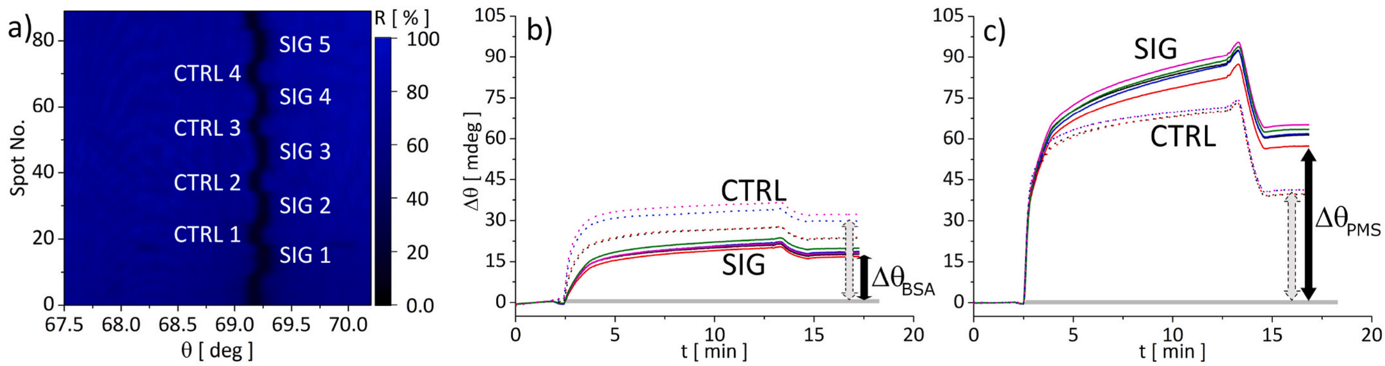

Fig. 2. (a) LF angular reflectance spectrum recorded in PBS 1 × at the beginning of an assay. The regions where the HER2-Fc chimera was incubated (SIG 1–5) can be clearly distinguished from the bare regions (CTRL 1–4). (b) LF sensogram recorded during the blocking step (v) and (c) during the sample injection step (vi), for an assay carried out with a negative sample. The dashed and solid curves are the mean curves recorded in the CTRL and SIG regions, respectively.

interactions between the sample and the biofunctionalized surface, the five SIG regions with HER2 were alternated with CTRL regions where BSA ensured an inert behavior after the blocking step. At this stage the biochip is ready for the competitive assay and, in a practical application, all the preliminary steps we described up to now can be carried out off-line on a large number of biochips at the same time.

In the competitive assay, a volume of 180 μL of the pre-mixed solution (PMS, sample + detection IgG*) is injected and incubated for 10 min, followed by a washing step with PBS 1 × . In Fig. 2c, we show the LF sensograms recorded during the injection/incubation for the SIG and CTRL regions for an assay carried out with a HER2-negative sample. At the end of such single determinant bioassay, the LF sensogram provides the angular residual shift associated to the sample reaction, $\Delta\theta_{PMS}$. As already mentioned above, the full scale of such a bioassay is reached in the case of HER2-negative samples. The unreacted detection-IgG* in the pre-mixed sample interacted preferentially with the SIG regions where the HER2 was present.

In Fig. 3, we focus the attention, for an assay carried out with a HER2-negative sample, on a restricted region of interest of the CCD image including just two adjacent SIG and CTRL regions. Fig. 3 a and c are portions of the CCD images collected in the LF and FLR mode, respectively. In Fig. 3 b and d, we plot the corresponding time resolved sensograms and endpoint fluorescence angular spectral density curves, respectively. The FLR spectra recorded at the end of the assay were background corrected by subtracting the background spectra FLR BGD recorded before injecting the pre-mixed sample into the microfluidic cell (indicated in Fig. 3a) and averaged in the SIG and CTRL regions. With reference to Fig. 3d, it is noteworthy that the angular emission spectra of the fluorophores can be decomposed into the TE and TM polarization components, in agreement with the surface modes (λ,θ) dispersion curve of the two polarization states [48,49]. By integrating the background subtracted angular emission spectra gathered during the experiments, we obtained the fluorescence emission intensity I.

The competitive assay protocol requires a preliminary optimization of two parameters mainly: the concentration of the HER2 solution (ζ_c) to be used for the bioconjugation step to maximize the avidity of the surface to the detection-IgG*, and the concentration of the detection-IgG* (ζ_d) to incubate with the sample.

3.2. Optimization of the competitive bioassay protocol

In this section, we report on the results of the optimization of the

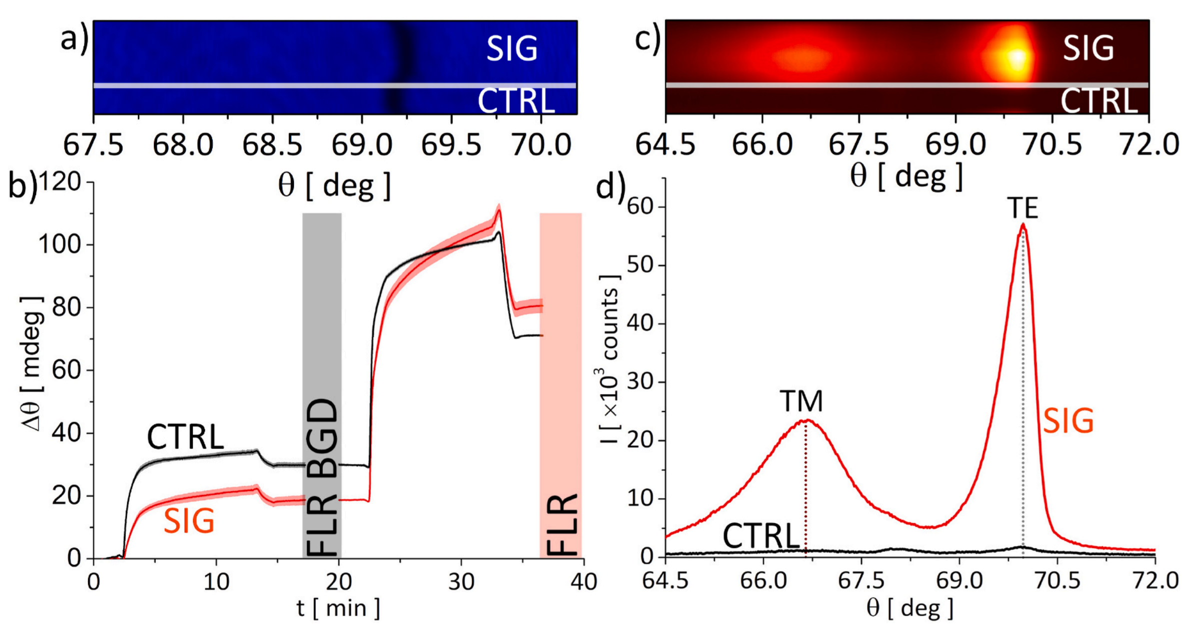

Fig. 3. (a) Portion of the collected LF reflectance spectra at the starting point of the bioassay. The larger number of molecules in the SIG region moves the BSW resonance to larger angles with respect to CTRL region. (b) LF time-dependent sensogram for experiment monitoring. (c) 2D collection of fluorescence emitted spectra showing spatial confinement between the SIG and the CTRL region. (d) Fluorescence intensity curves from SIG and CTRL areas.

parameters ζ_c and ζ_d carried out by exploiting the negative samples. The list of the assays carried out with different biochips are summarized in Table 1. Biochips 1 and 2 were used to test two values of ζ_c, while biochips 3 to 6 were used to determine the optimal ζ_d value. The biochip 7 and 8 were used to probe the two positive samples.

3.2.1. Optimization of ζ_c

To investigate the parameter ζ_c, we performed assays with two different biochips that were bio-conjugated by printing either 20 μg/mL or 100 μg/mL (biochip 1 and 2). The analysis of the resulting LF and FLR signals are plotted in Fig. 4. In panels a) and b), we plot the average LF residual angular shift in the different regions $\Delta\theta_{BSA}$ (after the step v) and $\Delta\theta_{PMS}$ (after the PMS injection, step vi), respectively. Data shown in Fig. 4a can be analyzed by defining the mean differential shift due to BSA binding for each neighbouring SIG and CTRL regions as:

$$\overline{\Delta\theta}_{BSA}^{DIF} = \overline{\Delta\theta_{BSA}^{DIF,j}} = \overline{\Delta\theta_{BSA}^{SIG,j} - \Delta\theta_{BSA}^{CTRL,j}} \tag{1}$$

where the index j stays for the SIG and CTRL spot pair number. The resulting values, which are listed in Table 1, demonstrate that, for both ζ_c values, a larger amount of BSA bound to the CTRL areas. Such a result validates the hypothesis that HER2 was correctly bio-conjugated onto the biochip, leading to a reduction in the number of binding sites accessible.

The bar plot of the residual $\Delta\theta_{PMS}$ in Fig. 4b, demonstrates the differential reactivity of the biochip regions upon the injection of the pre-mixed sample, with a differential residual shift:

$$\Delta\theta_{PMS}^{DIF,j} = \Delta\theta_{PMS}^{SIG,j} - \Delta\theta_{PMS}^{CTRL,j} \tag{2}$$

The resulting values are plotted in the bar plot shown in Fig. 4c.

The results of the LF assays are confirmed by the end-point FLR assays. Fig. 4d shows that the differential fluorescence intensities $I_{FLR}^{DIF,j}$, calculated as the difference of the background corrected intensities measured in neighbouring SIG and CTRL regions, show values that increase by a factor about 12, when passing from $\zeta_C = 20\ ng/mL$ to $\zeta_C = 100\ ng/mL$.

Fig. 4e reports the results for differential signals. Such signals are averaged over the five SIG regions for both the LF and the FLR operating modes, i.e., the $\overline{\Delta\theta}_{PMS}^{DIF}$ and $\overline{I}_{FLR}^{DIF}$ and listed in Table 1 for both biochips 1 and 2. Ultimately, to achieve a wider dynamic range with both LF and FLR modes, the working point of ζ_c was established at 100 μg/mL, taking into account that a negative sample is expected to produce a full-scale signal in the case of competitive bioassays.

3.2.2. Optimization of ζ_d

On the other hand, concentration of the detection-IgG*, ζ_d, requires to be calibrated in order to allow to the detection-IgG* to be completely segregated when it is let to react with the most concentrated HER2-positive sample. However, the positivity level of a sample is obviously a priori unknown. Hence, a set of detection-IgG* concentrations was preliminary tested on two types of samples within a fixed dynamic range of HER2 content. Four concentrations of detection-IgG* (1 nM, 2 nM, 5 nM and 10 nM) were tested with different biochips (from number 3 to 6, respectively) when injecting spiked HER2-positive plasmas. Moreover, two concentrations of detection IgG* (1 nM and 2 nM) were tested with two different biochips (7 and 8, respectively) when injecting an HER2-negative plasma. The LF and FLR results are shown in Fig. 5.

Similar to the ζ_C case, by using Eq. (2), we evaluated the $\Delta\theta_{PMS}^{DIF,j}$ values for each neighbouring SIG and CTRL regions during the LF part of the assay and the corresponding end-point fluorescence intensities $I_{FLR}^{DIF,j}$. In Fig. 5, for each bioassay, we show the resulting box plot. Here, the empty square dot represents the values of $\overline{\Delta\theta}_{PMS}^{DIF}$ and $\overline{I}_{FLR}^{DIF}$, for the LF and FLR cases, respectively. The grey (POS) and red (NEG) boxes mark the standard error of the mean, and the solid line inside the boxes represents the median. The crosses indicate the maximum and minimum values by $\Delta\theta_{PMS}^{DIF,j}$ and $I_{FLR}^{DIF,j}$ among the 5 couples of regions. Additionally, we plot the $1.5 \bullet IQR$ interval, where the parameter IQR has been carried out by means of the interquartile range (IQR) method [50]. To create this fence, we took 1.5 times the IQR and then subtracted this value from the first quartiles, Q_1, and added it to the third quartiles, Q_3. This approach helped us define the minimum and maximum fence posts to which we compare each observation. Any observations that are more than $1.5 \bullet IQR$ below Q_1 or more than $1.5 \bullet IQR$ above Q_3 can be considered *outliers*.

With reference to the boxplots of Fig. 5, the HER2-positive sample pre-mixed at $\zeta_d = 1\ nM$ remained unsorted by both operation modes. Instead, the HER2-positive sample pre-mixed at $\zeta_d = 2\ nM$ was successfully discriminated in the FLR mode only (complementary signal), confirming the FLR mode larger sensitivity, as mentioned above [43, 44]. Moreover, by observing the solid lines in figure, in the LF case, we can notice that the normal distribution of the data gets narrower when the number of molecules which are available for reaction on the biochip surface increases ($\zeta_d = 10\ nM$ and NEG case). Conversely, in the FLR case, the normal distribution spreads when a larger number of fluorescent molecules are bound at the biochip surface ($\zeta_d = 10\ nM$ and POS case; $\zeta_d = 2\ nM$ and NEG case). It is noteworthy that both the LF and FLR signals recorded in the assays performed with HER2-positive samples (black boxes in Fig. 5a and b) likely increase monotonically within the range of concentrations tested.

The presented approach wants to pave the way to systematic experimental sessions involving naturally positive and negative samples from breast cancer patients. Indeed, the proposed technique, can provide new insights in molecular understanding and proper identification

Table 1
List of the performed assays carried out with different biochips. The green boxes mark the optimal value for ζ_c and ζ_d.

Chip No.	Sample	ζ_c [$\mu g/mL$]	ζ_d [nM]	$\overline{\Delta\theta}_{BSA}^{DIF}$ [$mdeg$]	$\overline{\Delta\theta}_{PMS}^{DIF}$ [$mdeg$]	$\overline{I}_{FLR}^{DIF}$ [$\times 10^6\ counts$]
1	NEG	20	10	-24.1±5.3	-0.12±0.9	1.6±0.8
2		100	10	-9.3±0.8	21.3±1.4	29.6±1.7
3	POS	100	1	-44.8±2.6	-0.59±1.6	4.2±1.0
4		100	2	-49.5±1.2	1.98±0.6	9.5±1.6
5		100	5	-45.3±3.1	7.2±0.9	5.1±1.8
6		100	10	-43.4±2.5	19.1±1.6	19.4±1.2
7	NEG	100	1	-51.2±0.7	0.6±0.7	4.4±1.2
8		100	2	-55.8±2.3	-1.7±1.0	27.0±5.1

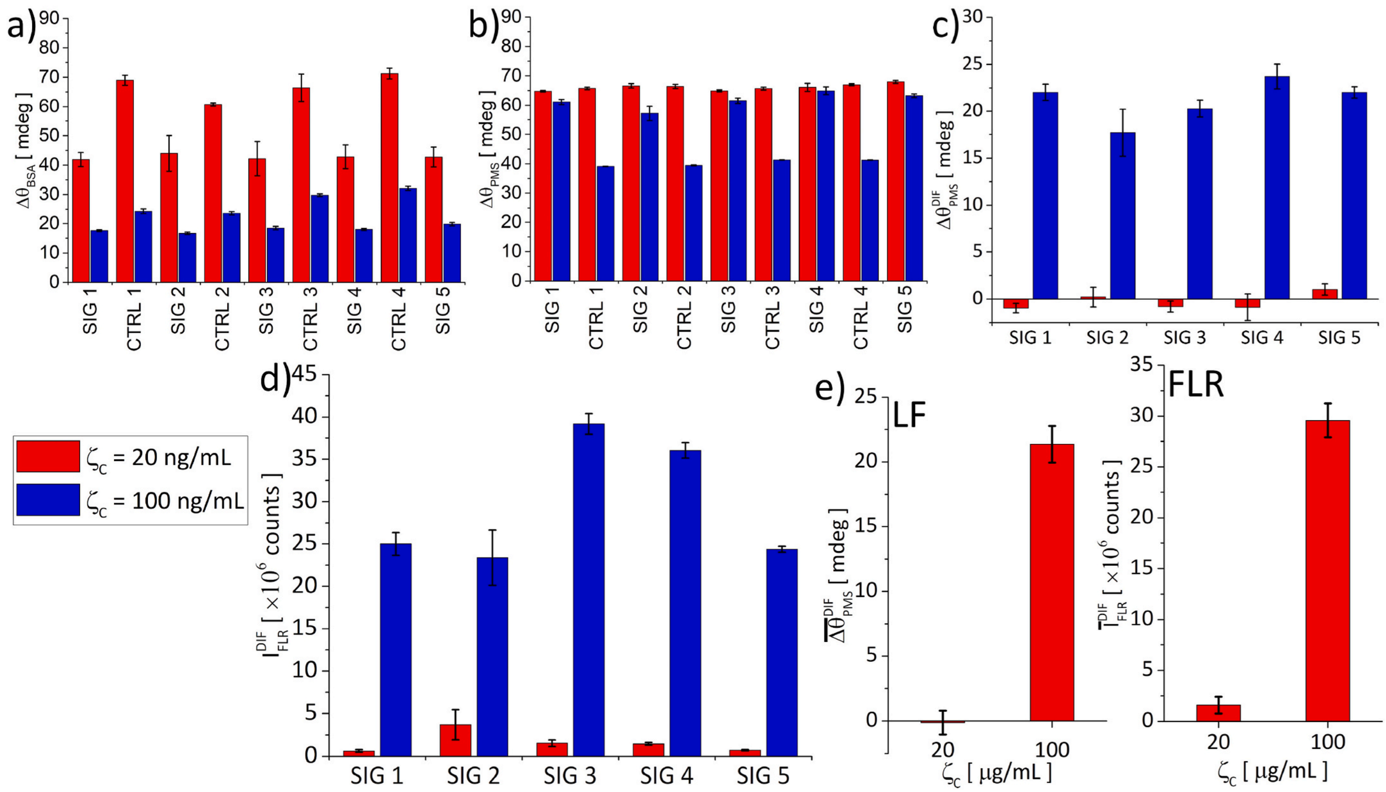

Fig. 4. Bar plots of the values of $\Delta\theta_{BSA}$ (a) and $\Delta\theta_{PMS}$ (b) recorded in each SIG and CTRL regions for a n assay carried out with a HER2-negative sample. The blue and red bars correspond to data obtained for $\zeta_c = 20\ ng/mL$ and $\zeta_c = 100\ ng/mL$, respectively. (c) Bar plot of the values of the $\Delta\theta_{res}$ in the SIG regions, extracted from data shown in (a) and (b). (d) The graph shows the fluorescence intensities in SIG regions after background subtraction. (e) The bar chart summarizes the average LF residual shifts $\overline{\Delta\theta}^{DIF}_{PMS}$ and emitted fluorescence intensities $\overline{I}^{DIF}_{FLR}$ for the two HER2 concentrations used in the bioconjugation process.

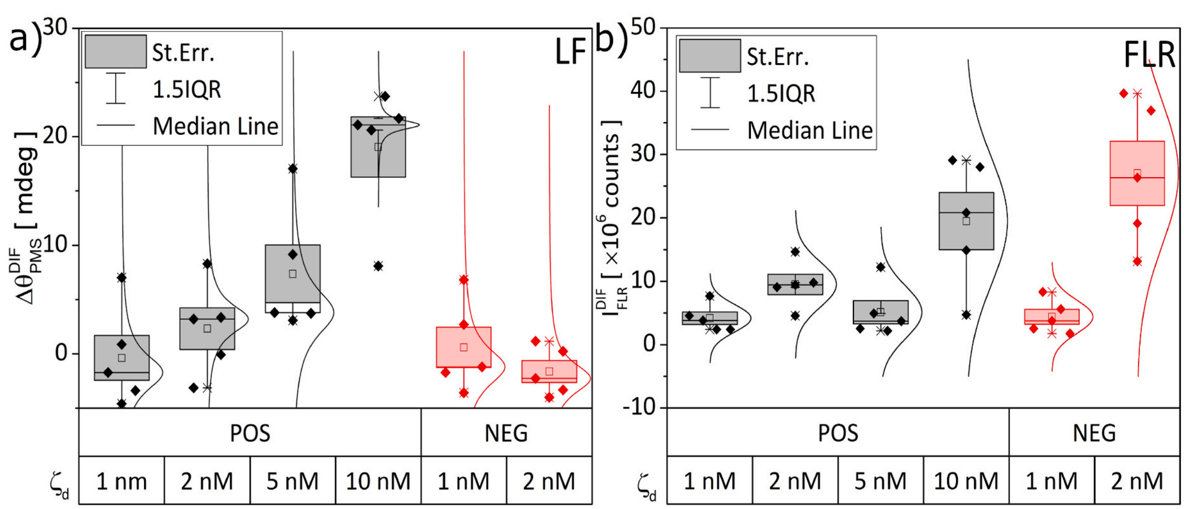

Fig. 5. (a) The LF residual shifts, $\Delta\theta^{DIF}_{PMS}$, and (b) emitted fluorescence, I^{DIF}_{FLR}, were measured at ζ_d concentrations of 1 nM, 2 nM, 5 nM, and 10 nM in positive (black) and negative (red) samples. The box plot shows the median (middle bar), the first quartile (lower bar), and the third quartile (upper bar) of the data. The whiskers extend to 1.5 times the IQR. The average values ($\overline{\Delta\theta}^{DIF}_{PMS}$ and $\overline{I}^{DIF}_{FLR}$) are represented by empty square dots, and the $\Delta\theta^{DIF,j}_{PMS}$ and $I^{DIF,j}_{FLR}$ values for each SIG region are represented by black diamond dots. The solid lines indicate the normal distribution of the data.

of breast cancer biomarkers in liquid biopsy applications from cancer patients.

3.3. Competitive assays with human plasma samples

In Fig. 6a, we show the 2D fluorescence maps recorded at the end of the assays for the following three 1:10 diluted human plasma samples: one HER2 positive sample (pt#13, ELISA quantification 16.3 ng/mL) and two negative samples (N1 and N2 from a pool of negative patients, ELISA quantification 0.9 ng/mL). By analysing the 2D fluorescence maps, we extracted the box plot shown in Fig. 6b where the solid spheres represent the average FLR intensity values measured in the SIG regions and their standard error, respectively.

As shown in Fig. 6b, the HER2-positive plasma sample pt#13 shows

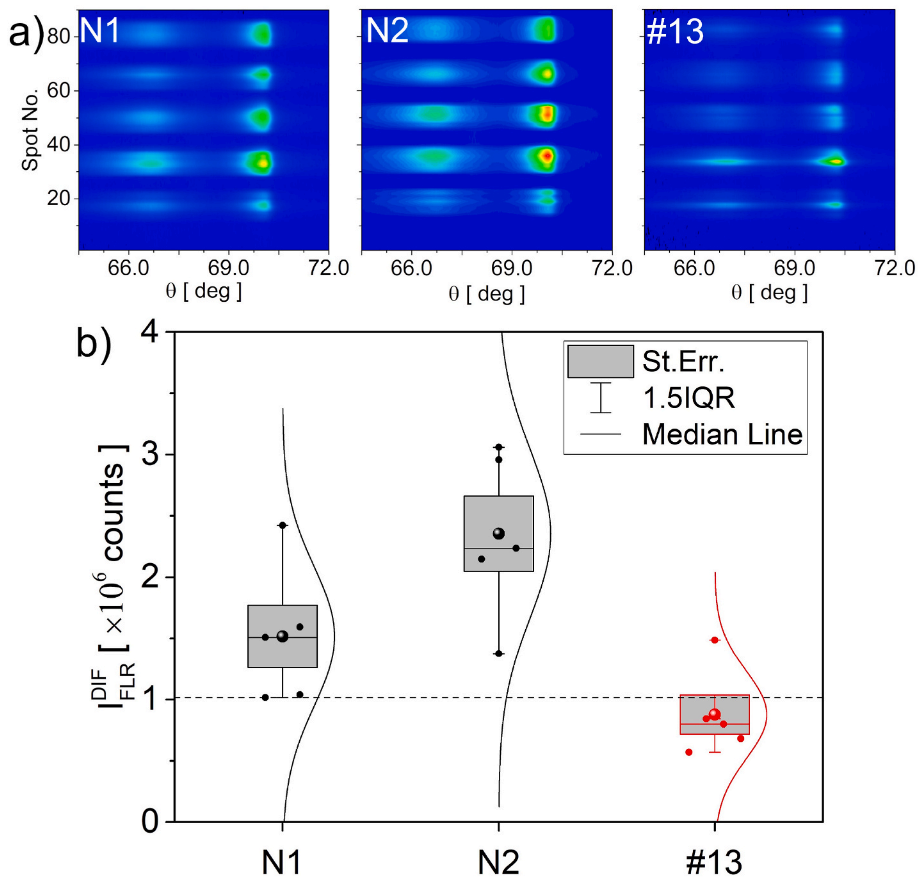

Fig. 6. a) 2D fluorescence maps obtained with the human plasma samples 1:10 from a pool of HER2-negative patients (N1 and N2) and from a HER2-positive patient (pt#13). b) Box plot of the integrated fluorescence intensity.

smaller fluorescence intensity with respect to the N1 and N2 samples, in particular, the average fluorescence intensity is below the 1.5IQR of the sample N1. Indeed, HER2-positive plasma samples typically exhibit increased expression of the HER2 protein, which can lead to enhanced interaction with the detection-IgG* reducing the binding of such antibodies onto the surface. As a result, lower fluorescence intensity is collected in HER2-positive samples, indicating a stronger interaction between the detection-IgG* and the target protein. Thus, even for natural plasma samples, the platform, operating in fluorescence mode, has the capability to generate distinct outputs when analyzing natural human plasmas based on their HER2 status.

4. Conclusions

In conclusion, the working parameters of a single determinant competitive assay were optimized to enable the biosensor for HER2 positivity assessment on diluted human plasma samples by means of BSW based sensors. It is worth noting that the overall running time of the direct competitive bioassay is 20 min only instead of 40 min required for the sandwich assay presented in Ref. [43]. This feature reduces dramatically the duration of the bioassay providing a sensitive and cost-effective alternative to the non-competitive methodologies. Even further, attention should be put on the duration when compared to other gold standard techniques such as ELFA/ELISA timescale that spans in the range of hours (4–8 h). Moreover, the LoD of commercial ELISA kits on purified recombinant HER2 that are routinely used in our laboratories is 1 ng/mL. By operating in fluorescence mode, the platform has demonstrated the capability to generate distinct outputs when analyzing natural human plasmas based on their HER2 content. The proposed approach can differentiate between plasma samples with different levels of HER2 in a relatively short time frame of 20 min. This rapid analysis time is advantageous in the clinical setting as it contributes to speeding up the detection of circulating biomarkers, specifically HER2 in this case.

Institutional review board statement

Healthy blood donors signed informed consent as per Regina Elena Ethical Review Board (IRB CEC/707/15).

CRediT author statement

The manuscript was written through contributions of all authors.

Tommaso Pileri: conceptualization, methodology, validation, investigation, writing—original draft preparation. **Alberto Sinibaldi**: conceptualization, methodology, validation, investigation, writing—original draft preparation, supervision, project administration, funding acquisition. **Agostino Occhicone**: methodology, software, validation, formal analysis, investigation, data curation, writing—original draft preparation. **Norbert Danz**: methodology, software, writing - review & editing. **Elena Giordani**: conceptualization, preparation of serum samples, resources. **Matteo Allegretti**: conceptualization, resources, writing - review & editing, supervision. **Frank Sonntag**: methodology, resources. **Peter Munzert**: 1D-Photonic Crystals fabrication. **Patrizio Giacomini**: methodology, investigation, conceptualization, resources, writing - review & editing, supervision. **Francesco Michelotti**: conceptualization, methodology, software, resources, writing - review & editing, supervision, project administration, funding acquisition.

Declaration of competing interest

The authors declare that they have no known competing financial interests or personal relationships that could have appeared to influence the work reported in this paper.

Data availability

Data will be made available on request.

Acknowledgements

A.O. acknowledges funding from the project BIOLIGHT (B86J20001690002), F.M. from the projects NANO-COVID-TEST (A0375-2020-36528) and PNRR-PNC-D34Health (B53C22006120001), A.S. from the projects ERBB2-2D (A0375-2020-36630), and PNRR-Rome Technopole Flagship Project 7 (B83C22002820006). The authors wish to thank Paola Di Matteo for her assistance on the chemical functionalization of the biochips, and Marco Magi for technical assistance.

References

[1] A.M.S. Berghuis, H. Koffijberg, J. Prakash, L.W.M.M. Terstappen, M.J. Ijzerman, Detecting blood-based biomarkers in metastatic breast cancer: a systematic review of their current status and clinical utility, Int. J. Mol. Sci. 18 (2) (2017) 363.
[2] M.H. Son, S.W. Park, H.Y. Sagong, Y.K. Jung, Recent advances in electrochemical and optical biosensors for cancer biomarker detection, BioChip J. 17 (2022) 44–67.
[3] X. Lu, C. Yao, L. Sun, Z. Li, Plasmon-enhanced biosensors for microRNA analysis and cancer diagnosis, Biosens. and Bioelectr. 203 (2022), 114041.
[4] S.D. Choudhury, R. Badugu, J.R. Lakowicz, Directing fluorescence with plasmonic and photonic structures, Acc. Chem. Res. 48 (2015) 2171–2180.
[5] A. Sinibaldi, Cancer biomarker detection with photonic crystals-based biosensors: an overview, J. Lightwave Technol. 39 (12) (2021).
[6] R. Badugu, K. Nowaczyk, E. Descrovi, J.R. Lakowicz, Radiative decay engineering 6: fluorescence on one-dimensional photonic crystals, Anal. Biochem. 442 (2013) 83–96.
[7] P.C. Mathias, N. Ganesh, B.T. Cunningham, Application of photonic crystal enhanced fluorescence to a cytokine immunoassay, Anal. Chem. 80 (23) (2008) 9013–9020, 2008.
[8] M.M. Abadla, H.A. Elsayed, Detection and sensing of hemoglobin using one-dimensional binary photonic crystals comprising a defect layer, Appl. Opt. 59 (2) (2020) 418–424.
[9] B.T. Cunningham, R.C. Zangar, Photonic crystal enhanced fluorescence for early breast cancer biomarker detection, J. Biophot. (2012).
[10] C.S. Huang, S. George, M. Lu, V. Chaudhery, R. Tan, R.C. Zangar, B. T. Cunningham, Application of photonic crystal enhanced fluorescence to cancer biomarker microarrays, Anal. Chem. 83 (4) (2011) 1425–1430.
[11] R. Rizzo, M. Alvaro, N. Danz, L. Napione, E. Descrovi, S. Schmieder, A. Sinibaldi, S. Rana, R. Chandrawati, P. Munzert, T. Schubert, E. Maillart, A. Anopchenko, P. Rivolo, A. Mascioletti, E. Förster, F. Sonntag, M. Stevens, F. Bussolino, F. Michelotti, Bloch surface wave enhanced biosensor for the direct detection of Angiopoietin-2 tumor biomarker in human plasma, Biomed. Opt Express 9 (2) (2018) 529–542.
[12] A. Sinibaldi, N. Danz, E. Descrovi, P. Munzert, U. Schulz, F. Sonntag, L. Dominici, F. Michelotti, Direct comparison of the performance of Bloch surface wave and surface plasmon polariton sensors, Sens. Actuators, B 174 (2012).
[13] Y. Guo, C. Divin, A. Myc, F.L. Terry, J.R. Baker, T.B. Norris, J. Yong Ye, Sensitive molecular binding assay using a photonic crystal structure in total internal reflection, Opt Express 16 (16) (2008) 11741–11749.
[14] M. Shinn, W.M. Robertson, Surface plasmon-like sensor based on surface electromagnetic waves in a photonic band-gap material, Sensor. Actuator. B Chem. 105 (2005) 360–364.
[15] W.M. Robertson, S.M. Wright, A. Friedli, J. Summers, A. Kaszynski, Design and Characterization of an Ultra-low-cost 3D-Printed Optical Sensor Based on Bloch Surface Wave Resonance, vol. 5, Biosens Bioelectron X, 2020.
[16] B. Kalas, K. Ferencz, A. Saftics, Z. Czigany, M. Fried, P. Petrik, Bloch surface waves biosensing in the ultraviolet wavelength range – bragg structure design for investigating protein adsorption by in situ Kretschmann-Raether ellipsometry, Appl. Surf. Sci. 536 (2021).
[17] M. Gryga, D. Ciprian, L. Gembalova, P. Hlubina, Sensing based on Bloch surface wave and self-referenced guided mode resonances employing a one-dimensional photonic crystal, Opt Express 29 (9) (2021) 12996–13010.
[18] G.N. Sharma, R. Dave, J. Sanadya, P. Sharma, K.K. Sharma, Various types and management of breast cancer: an overview, J Adv. Pharm. Technol. Res. 1 (2) (2010) 109–126.
[19] A. Milani, D. Sangiolo, F. Montemurro, M. Aglietta, G. Valabrega, Active immunotherapy in HER2 overexpressing breast cancer: current status and future perspectives, Ann. Oncol. 24 (2013) 1740–1748.
[20] C. Tsé, A.S. Gauchez, W. Jacot, P.J. Lamy, HER2 shedding and serum HER2 extracellular domain: biology and clinical utility in breast cancer, Lab.-Clinic Inter. 38 (2) (2012) 133–142.
[21] D. Di Gioia, M. Dresse, D. Mayr, D. Nagel, V. Heinemann, P. Stieber, Serum HER2 in combination with CA 15-3 as a parameter for prognosis in patients with early breast cancer, Clin. Chim. Acta 440 (2) (2015) 16–22.
[22] E. Arkan, R. Saber, Z. Karimi, M. Shamsipur, A novel antibody–antigen based impedimetric immunosensor for low level detection of HER2 in serum samples of breast cancer patients via modification of a gold nanoparticles decorated multiwall carbon nanotube-ionic liquid electrode, Anal. Chim. Acta 874 (18) (2015) 66–74.
[23] Z. Zhang, C. Li, H. Fan, Q. Xiang, L. Xu, Q. Liu, S. Zhou, Q. Xie, S. Chen, G. Mu, Y. Cui, Prognostic value of baseline serum HER2 extracellular domain level with a cut-off value of 15 ng/mL in patients with breast cancer: a systematic review and meta-analysis, Breast Cancer Res. Treat. 172 (3) (2018) 513–521.
[24] T.A. Christianson, J.K. Doherty, Y.J. Lin, E.E. Ramsey, R. Holmes, E.J. Keenan, G. M. Clinton, NH2-terminally truncated HER-2/neu protein: relationship with shedding of the extracellular domain and with prognostic factors in breast cancer, Cancer Res. 58 (22) (1998) 5123–5129.
[25] A. Perrier, J. Gligorov, G. Lefèvre, M. Boissan, The extracellular domain of Her2 in serum as a biomarker of breast cancer, Lab. Invest. 98 (6) (2018) 696–707.
[26] W.P. Carney, D. Bernhardt, B. Jasani, Circulating HER2 extracellular domain: a specific and quantitative biomarker of prognostic value in all breast cancer patients? Biomarkers Cancer 5 (2013).
[27] S. Eppenberger-Castori, D. Klingbiel, T. Ruhstaller, D. Dietrich, D.A. Rufle, K. Rothgiesser, O. Pagani, B. Thürlimann, Plasma HER2ECD a promising test for patient prognosis and prediction of response in HER2 positive breast cancer: results of a randomized study - SAKK 22/99, BMC Cancer 20 (114) (2020).
[28] S. Eppenberger-Castori, W. Kueng, C. Benz, R. Caduff, Z. Varga, F. Bannwart, D. Fink, H. Dieterich, M. Hohl, H. Müller, K. Paris, F. Schoumacher, U. Eppenberger, Prognostic and predictive significance of ErbB-2 breast tumor levels measured by enzyme immunoassay, J. Clin. Oncol. 19 (3) (2001) 645–656.
[29] A. Sinibaldi, C. Sampaoli, N. Danz, P. Munzert, F. Sonntag, F. Centola, A. Occhicone, E. Tremante, P. Giacomini, F. Michelotti, Bloch surface waves biosensors for high sensitivity detection of soluble ERBB2 in a complex biological environment, Biosensors 7 (3) (2017).
[30] J.D. Joannopoulos, S.G. Johnson, J.N. Winn, R.D. Meade, Photonic Crystals: Molding the Flow of Light, Princeton University press, Princeton and Oxford, 2008.
[31] M. Ballarini, F. Frascella, N. De Leo, S. Ricciardi, P. Rivolo, P. Mandracci, E. Enrico, F. Giorgis, F. Michelotti, E. Descrovi, A polymer-based functional pattern on one-dimensional photonic crystals for photon sorting of fluorescence radiation, Opt Express 20 (6) (2012) 6703–6711.
[32] P. Yeh, A. Yariv, C.S. Hong, Electromagnetic propagation in periodic stratified media. I. General theory, J. Opt. Soc. Am. 67 (1977) 423–438.
[33] R. Rizzo, M. Alvaro, N. Danz, L. Napione, E. Descrovi, S. Schmieder, A. Sinibaldi, R. Chandrawati, S. Rana, P. Munzert, T. Schuberth, E. Maillart, A. Anopchenko, P. Rivolo, A. Mascioletti, F. Sonntag, M.M. Stevens, F. Bussolino, F. Michelotti, Bloch surface wave label-free and fluorescence platform for the detection of VEGF biomarker in biological matrices, Sens. Actuators, B 255 (2018) 2143–2150.
[34] P. Rouquette, C. Amra, M. Zerrad, M. Lequime, Micro-cavity optimization for ultra-sensitive all-dielectric optical sensors, Opt Express 30 (9) (2022) 15344–15364.
[35] P. Hlubina, M. Gryga, D. Ciprian, P. Pokorny, L. Gembalova, J. Sobota, High performance liquid analyte sensing based on Bloch surface wave resonances in the spectral domain, Opt Laser. Technol. 145 (2022), 107492.
[36] J.Y. Ye, M. Ishikawa, Y. Yamane, N. Tsurumachi, H. Nakatsuka, Enhancement of two-photon excited fluorescence using one-dimensional photonic crystals, Appl. Phys. Lett. 75 (1999) 3605–3607.
[37] J.Y. Ye, M. Ishikawa, Enhancing fluorescence detection with a photonic crystal structure in a total-internal-reflection configuration, Opt. Lett. 33 (2008) 1729–1731.
[38] M. Liscidini, M. Galli, M. Shi, G. Dacarro, M. Patrini, D. Bajoni, J.E. Sipe, Strong modification of light emission from a dye monolayer via Bloch surface waves, Opt. Lett. 34 (2009) 2318–2320.
[39] L. Lam, N. McAndrew, M. Yee, T. Fu, J.C. Tchou, H. Zhang, Challenges in the clinical utility of the serum test for HER2 ECD, Biochim. Biophys. Acta 1826 (1) (2012) 199–208.
[40] F. Michelotti, R. Rizzo, A. Sinibaldi, P. Munzert, C. Wächter, N. Danz, Design rules for combined label-free and fluorescence Bloch surface wave biosensors, Opt. Lett. 42 (14) (2017) 2798–2801.
[41] P. Munzert, N. Danz, A. Sinibaldi, F. Michelotti, Multilayer coatings for Bloch surface wave optical biosensors, Surf. Coat. Technol. 314 (2017) 79–84.
[42] E. Kretschmann, H. Raether, Radiative decay of non radiative surface plasmons excited by light, Z. Naturforsch. 23 (1968) 2135–2136.
[43] A. Sinibaldi, A. Doricchi, T. Pileri, M. Allegretti, N. Danz, P. Munzert, E. Giordani, P. Giacomini, F. Michelotti, Bioassay engineering: a combined label-free and fluorescence approach to optimize HER2 detection in complex biological media, Anal. Bioanal. Chem. 412 (14) (2020).
[44] A. Sinibaldi, A. Fieramosca, R. Rizzo, A. Anopchenko, N. Danz, P. Munzert, C. Magistris, C. Barolo, F. Michelotti, Combining label-free and fluorescence operation of Bloch surface wave optical sensors, Opt. Lett. 39 (10) (2014) 2947–2950.
[45] N. Siva, K. Gunda, M. Singh, L. Norman, K. Kaur, S.K. Mitra, Applied Surface Science Optimization and characterization of biomolecule immobilization on silicon substrates using (3-aminopropyl) triethoxysilane (APTES) and glutaraldehyde linker, Appl. Surf. Sci. 305 (2014) 522–530.

[46] J.A. De Feijter, J. Benjamins, F.A. Veer, Ellipsometry as a tool to study the adsorption behaviour of synthetic and biopolymers at the air–water interface, Biopolymers 17 (1978) 1759–1772.
[47] J. Voros, The density and refractive index of adsorbing protein layers, Biophys. J. 87 (1) (2004) 553–561.
[48] F. Michelotti, E. Sepe, Anisotropic fluorescence emission and photobleaching at the surface of one-dimensional photonic crystals sustaining Bloch surface waves. I. Theory, J. Phys. Chem. C 123 (34) (2019) 21167–21175.
[49] E. Sepe, A. Sinibaldi, N. Danz, P. Munzert, F. Michelotti, Anisotropic fluorescence emission and photobleaching at the surface of one-dimensional photonic crystals sustaining Bloch surface waves. II. Experiments, J. Phys. Chem. C 123 (34) (2019) 21176–21184.
[50] A.P. King, R.J. Eckersley, Statistics for Biomedical Engineers and Scientists, Academic Press, 2019, pp. 23–56.